Liquid Infiltration into Carbon Nanotube Fibers: Effect on Structure and Electrical Properties

Jing Qiu,[§] Jeronimo Terrones,[§] Juan J. Vilatela,[†] Mary E. Vickers, James A. Elliott, and Alan H. Windle*

Department of Materials Science, University of Cambridge, 27 Charles Babbage Road, Cambridge, Cambridgeshire CB3 0FS, United Kingdom. [§]These authors made equal contributions to the work. All authors have given approval to the final version of the manuscript. [†]Present address: IMDEA Materials Institute, Eric Kandel 2, Getafe, Madrid 28906, Spain.

ABSTRACT Carbon nanotube (CNT) fibers consist of a network of highly oriented carbon nanotube bundles. This paper explores the ingress of liquids into the contiguous internal pores between the bundles using measurements of contact angles and changes in fiber dimensions. The resultant effects on the internal structure of the fiber have been examined by WAXS and SAXS. A series of time-resolved experiments measured the influence of the structural changes on the electrical resistivity of the fiber. All organic liquids tested rapidly wicked into the fiber to fill its internal void structure. The local regions in which the nanotube bundles are aggregated to give a bundle network were broken up by the liquid ingress. For the range of organic penetrants examined, the strength of the effects on structure and electrical resistivity was correlated, not only with the degree to which the liquid reduced the nanotube surface energy, but also with the Hansen affinity parameters. The fact that liquid environments influence the electrical performance of these fibers is of significance if they are to replace copper as power and signal conductors, with added implications regarding the possible ingress of external insulating materials, and possibly also sensing applications.

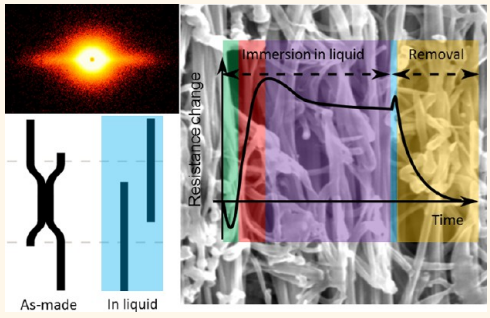

KEYWORDS: CNT fiber · electrical conductivity · liquid infiltration · small-angle X-ray scattering · structural model

Much of the original promise for fibers made from carbon nanotubes lay in the realm of mechanical properties spurred, initially, by the measurement of the strength of individual nanotubes in 2000 by Yu *et al.*[1,2] The values they obtained suggested that approximately 25 N tex^{-1} (numerically equal to 25 GPa divided by the specific gravity of fiber relative to water) might be expected for tensile strength, which is at least 5 times greater than any other available "high tech fiber". However, the challenge of achieving such values in a fiber assembly of carbon nanotubes remains. Various methods of making such fibers have emerged,[3−6] but for samples of lengths in excess of 1−2 cm, the maximum strengths seen so far are of the order of 1−2 N tex^{-1}, although much higher values, approaching 10 N tex^{-1}, have been reported for testing of shorter lengths of some fibers.[7] Carbon nanotube fibers have an inherently hierarchical structure with high internal surface area, that can approach 100 m^2 g^{-1}, which is contiguous and thus accessible to absorbed fluids. One approach to enhancing strength has been through the infiltration of material into the void content of the fiber, especially a monomer that could be subsequently cross-linked or otherwise polymerized.[8] More recently, with attention turning to the possible application of CNT fibers as electrical conductors, with the objective to achieve values that may eventually challenge copper, the possibility of infiltrating with a medium to enhance electron transport of the nanotube assembly has been the subject of recent experiments.[9,10]

The purpose of this paper is to describe studies of the mechanism and criteria for liquid absorption into CNT fiber and to apply X-ray scattering techniques to probe changes in the internal microstructure of the fiber. The influence of such ingress on the electrical properties of the fiber is also reported as a function of liquid type, with a focus on obtaining an enhanced

* Address correspondence to: ahw1@cam.ac.uk.

Received for review March 17, 2013 and accepted September 3, 2013.

Published online September 03, 2013
10.1021/nn401337m

understanding of the relationship between structure and properties, as a precursor to future work in which absorbed liquids will be turned into stable solids in the ongoing quest for greater strength and greater conductivity. The liquids chosen are all organic solvents, with a considerable range of polarities. They also include *N*-methyl-2-pyrrolidone (NMP), which is now established as one of the most powerful agents in the dispersion of carbon nanotubes.[11,12]

RESULTS AND DISCUSSION

Materials. CNT fibers used in this study were produced by the floating catalyst chemical vapor deposition (CVD) method.[6] Bearing in mind the possibility of some variance between different parts of the fiber in a given batch and of course between batches, we give here characterization data for one sample piece, which will be generally typical of all fibers examined. Fiber diameter: $14.8 \pm 1.4\ \mu$m, surface area: $75.6 \pm 0.7\ m^2\ g^{-1}$, and porosity: 54.4% (SOM 1 and 2 in Supporting Information). It also contains 17.3 wt % of carbonaceous impurities and 3.1 wt % iron particles (SOM 3 in Supporting Information), which are randomly distributed inside the fiber. The fibers consist of highly oriented CNT bundles separated by interbundle pores, both of which are aligned parallel to the fiber axis (Figures 1 and 2). Every bundle contains mainly collapsed double-wall nanotubes (DWNTs) with a "dog bone" cross section with dimension of the order of 10 nm × 1.5 nm and of lengths approximately 1 mm.[13,14] There are also some multiwalled nanotubes (MWNTs) and a small proportion of single wall nanotubes (SWNTs).

The diameters of the nanotube bundles and the interbundle pores can be characterized directly using the longitudinal section SEM images of the CNT fiber (Figures 2b and 3a), and the result indicates that the distribution of the bundle diameters is similar to that observed for interbundle pore diameters. Figure 3b shows that the distribution of bundle sizes peaks in the 20−30 nm range, while that of the pores reaches a maximum in the 30−40 nm range. While these measurements have been made on FIB-cut sections of the as-spun fiber, their extension to fibers containing liquids, some of which are quite volatile, presents significant additional difficulties. X-ray scattering measurements, both wide angle (WAXS) and small angle (SAXS), were thus employed to provide a relative indication of the effect of absorbed liquids on the characteristic dimensions of the microstructure. However, before discussing these results, we will first address the more macroscopic aspects of the absorption of a range of organic liquids by the fiber.

Wetting and Wicking. The contact angles of the various liquids with the nanotubes were measured by microscopic examination using a video camera (frame speed 25 s^{-1}) to record droplets in contact with

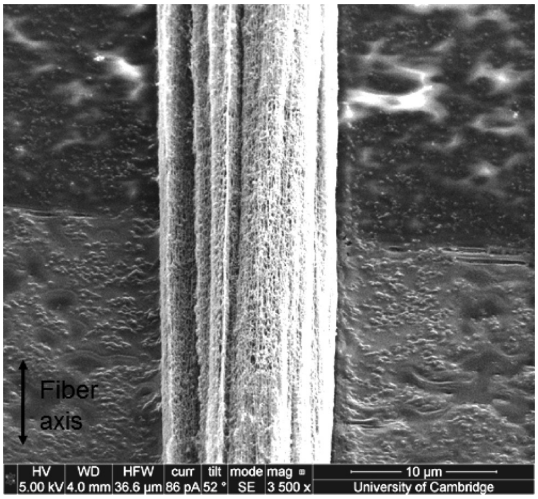

Figure 1. A SEM image of a CNT fiber.

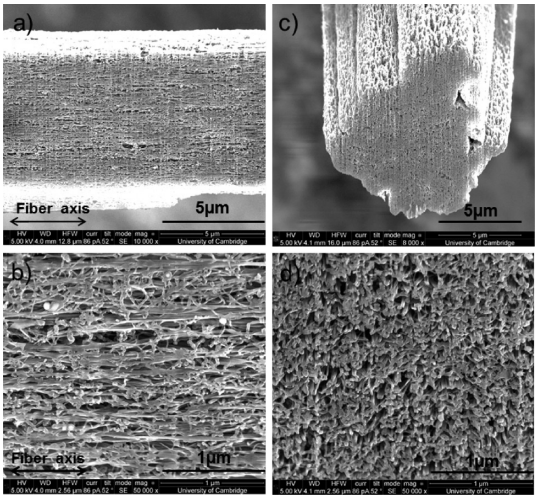

Figure 2. SEM images of a CNT fiber cut using a focused ion beam (FIB) showing the (a,b) longitudinal and (c,d) radial cross sections of the fiber.

aligned arrays of nanotube bundles that had not been condensed into a fiber (SOM 4 in Supporting Information). The contact angle data for the relevant liquids are shown in Figure 4a. With the exception of water, which does not wet the nanotubes, all the liquids spread rapidly across the surface at rates between 5 and 10 mm s^{-1}, as shown in the data of Figure 4b. The result of the wicking is that the contact angles appear to tend to 0° as the liquid is absorbed into the nanotube array and wetting rapidly becomes wicking. However, the extrapolation of the contact angle curves to $t = 0$, which gives an indication of the surface contact angle before penetration and wicking had been established. These zero time data are in Table 1, together with physical parameters of the liquid used.

Given that the surface energy (tension) of each of the liquids in air, and that of graphene, are known, the contact angle (θ) can be used to estimate a value for

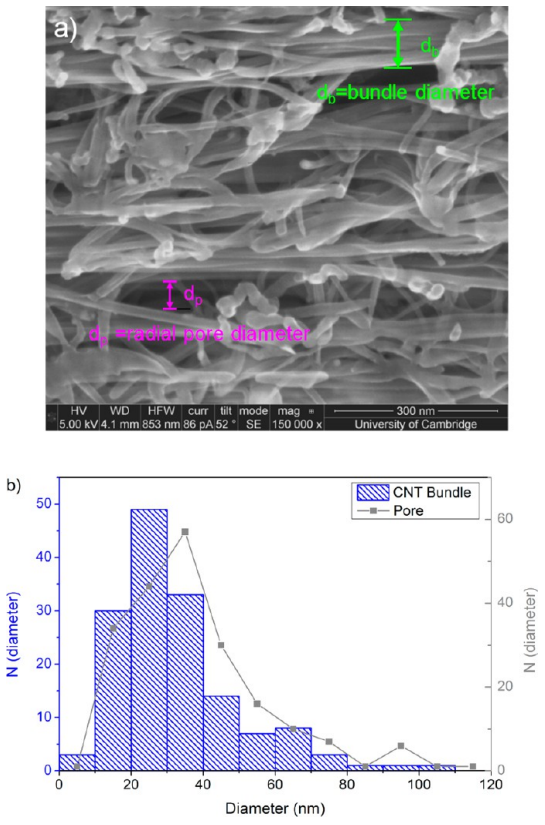

Figure 3. (a) A SEM image at a higher magnification of a FIB cut longitudinal section of a CNT fiber showing the inter-bundle pores and CNT bundles, and (b) histogram of the lateral bundle dimensions (blue columns) and pore dimensions (gray points).

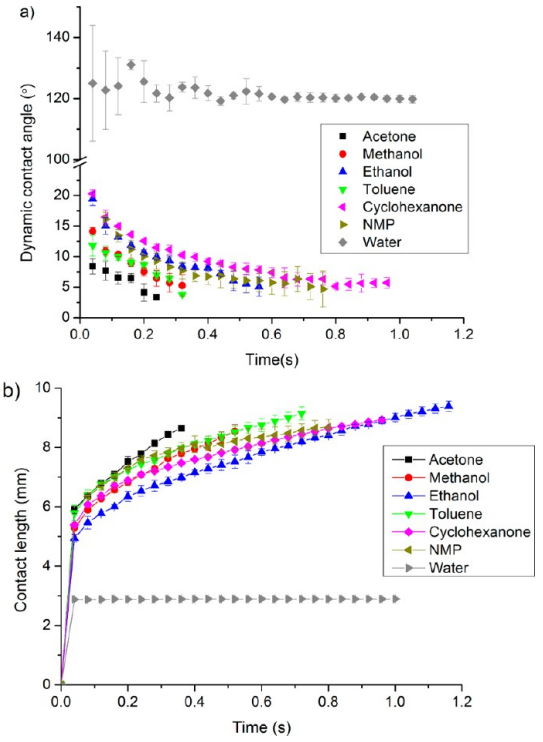

Figure 4. Diagrams showing the plot of (a) dynamic contact angle and (b) the contact length between the liquid and the CNT arrays with time.

the liquid−graphene interface energy from the relationship $\gamma_{s/l} = \gamma_{s/a} - \gamma_{l/a} \cos\theta$. Wicking does not change the area of the liquid−air interface, and thus the criterion for this process to occur is simply that $\gamma_{s/a} > \gamma_{s/l}$ and we may consider its driving force to be $\gamma_{s/a} - \gamma_{s/l}$ which is the parameter listed in Table 1. If we take the value given by Wang *et al.*[15] for the surface energy of graphene to be 47 mJ m^{-2}, then the values of $\gamma_{s/l}$ follow as listed in the final column of Table 1. We conclude that the organic liquids will rapidly wick within the fibers and fill the internal interconnecting voids such as those shown in Figure 2. Water neither wets nor wicks the fiber; however, the value of its contact angle with our CNT arrays is similar to, albeit at the high end, of published values for contact on the planar surfaces of graphitic materials[15,17] and thus validates our measurement procedure. This gives a measure of confidence that the "roughness" of the nanotube array surfaces does not have a major influence on the contact angle measurements. Water will not be considered further here, except for the observation that it does not wick and fill the fiber voids, which is also confirmed, in passing, by the SAXS measurments below.

Effect of Liquids on Fiber Dimensions. The radial swelling of a CNT fiber was quantified by microscopic observation of the diameter of the fiber both dry and after immersion. The measurement of the diameter of a yarn-like fiber is challenging because of its porous structure, which is why the unit of N tex^{-1} is often used for specific stress, as it requires no measurement of the cross-section. The rapid evaporation of some of the solvents also raised practical difficulties, so the measurements were not made on highly volatile solvents such as acetone. Nevertheless, considering just NMP and toluene, it was always possible to observe an increase in diameter on immersion, although the shift of the Gaussian peak fitted to the histogram of the fiber diameters on immersion (Figure 5b) was always less than the width of the distribution of diameters as measured along a given piece of as-made fiber (Figure 5a). There is also the issue as to whether some of the yarn elements were becoming loose at the surface, producing a nonuniform swelling. We summarize here that, working with samples swollen in NMP and toluene, we observed increases in diameter between 10 and 50%. Figure 5 shows the data for NMP.

Changes in the length of fiber on liquid infiltration were measured using a Favimat fiber tensile testing machine. The fiber was stressed to a predetermined level, and then, while held at constant extension, the liquid was added, which immediately wicked along the full fiber length. Figure 6a shows an example of the effect of adding a penetrant liquid, in this case, acetone, to the stressed fiber. There was an immediate drop in stress, indicating a sudden increase in length, which was not recovered as the acetone evaporated

TABLE 1. List of Physical Parameters for Various Liquids

liquid	density[16] (g cm^{-3})	vapor pressure[16] at 25 °C (kPa)	surface tension[16] (mN m^{-1}) at 1 atm at 25 °C	viscosity[16] (mPa s) at 25 °C	contact angle (t = 0) degree	$\gamma_{s/a} - \gamma_{s/l}$ (mN m^{-1})	$\gamma_{s/l}$ (mN m^{-1})
acetone	0.78	30.8	22.7	0.31	9.1	22.4	24.6
methanol	0.79	16.9	22.5	0.59	17.3	21.5	25.5
ethanol	0.79	7.9	22.0	1.1	23.9	20.1	26.9
toluene	0.87	3.8	27.7	0.56	13.0	27.0	20.0
cyclohexanone	0.95	0.53	34.6	2.0	24.1	31.5	15.4
NMP	1.02	0.04	40.2	1.7	21.5	37.4	9.6
water	1.00	3.2	72.0	0.89	127.3	−43.6	90.6

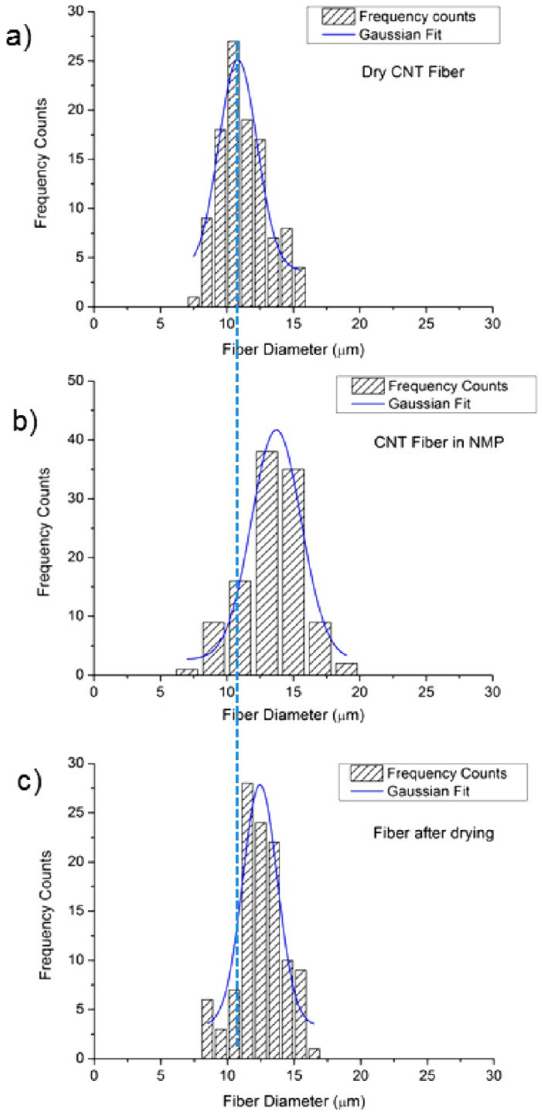

Figure 5. Distributions of fiber diameters for (a) as-made CNT fiber, (b) the same fiber in liquid NMP, and (c) dried at 120 °C for 20 min.

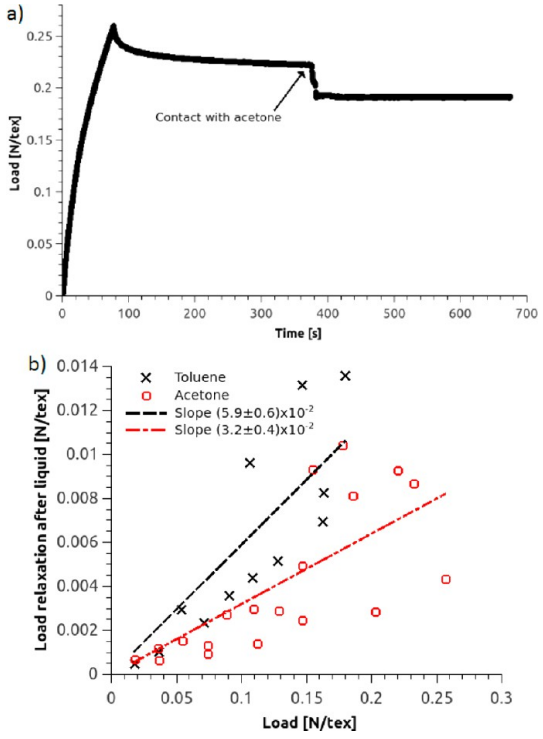

Figure 6. Plot of (a) change of load required to maintain a CNT fiber at a constant extension when an acetone droplet was brought in contact with the fiber and (b) penetrant induced load drop against the preapplied stress for acetone and toluene.

over a few seconds. However, when measurements of load drop were plotted against the actual load applied, they all extrapolated to zero, indicating that without load, there was no change in length on absorption. Figure 6b shows data for acetone and toluene. Each point is a separate sample, and the scatter is again the variability from sample to sample of the same batch. Measurements using NMP had to be curtailed, as the solvent was damaging the machine grip system; however, initial indications were in line with those for the other two liquids. The mechanical implications of these observations will not be considered further here.

We conclude that although the accessible void volume is filled on immersion in the liquid and there is some increase in fiber diameter (the exact amount is difficult to quantify), there is no change in fiber length in the absence of applied load. The question now remains as to the effect of the penetrating liquid on the internal organization of the yarn-like fibers, and for this we turn to X-ray scattering methods.

Wide Angle X-ray Scattering from Fibers with Penetrant. The possible intercalation of the organic liquids into

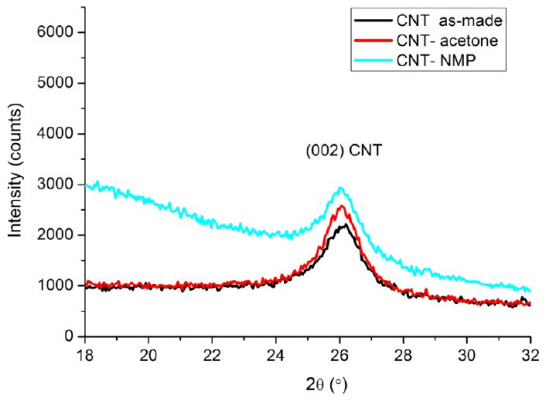

Figure 7. WAXS of an aligned array of CNT bundles before and after exposure to acetone and then NMP at room temperature. The increased background from the NMP experiment is due to residual liquid external to the fiber.

the CNT bundles was studied by WAXS. The 002 CNT reflection is caused by the scattering between the stacked graphene layers of collapsed nanotubes within the CNT bundles.[18,19] If there was intercalation of the liquid molecules in-between collapsed graphene layers within the CNT bundles, expansion of *d*-spacing between these layers should be detectable as a shifting of the position of the 002 peak to lower scattering angles. The data, Figure 7, show that there is no significant change in position of this peak and thus no evidence for molecules of a liquid inserting themselves between the (002) planes. Of course, there is possibility of the presence of multiwall nanotubes in the sample with sufficient layers to generate the 002 peaks observed, where it would not be surprising that the liquid does not intercalate between the layers.

Small Angle X-ray Scattering (SAXS). SAXS measures the difference in electron density (here, to a good approximation, just the mass density) between 2 phases and thus has been widely used to study fibers, both dry and immersed in liquids (see SOM 5 in Supporting Information).[20] Figure 8a shows a typical background-corrected SAXS pattern of as-made CNT fibers with collection time of 90 min using a Cu Kα radiation source (λ = 1.542 Å). It can be seen that a fiber streak is clearly visible and overlaps isotropic scattering. The fiber streak arises from aligned CNT bundles and the elongated interbundle pores, whereas the isotropic contribution is caused by the scattering from some unoriented CNT bundles and from impurities within the fiber, such as isotropic iron catalyst particles and multilayered graphitic impurities, randomly dispersed in the fiber.[18,19] The analysis has thus focused on the fiber streak, and Figure 8b shows plots of the fiber streak intensity for not only the as-made fibers but also fibers containing the absorbed liquids: acetone, ethanol, toluene, cyclohexanone, NMP and deionized water as a function of scattering vector *q* (defined as $4\pi \sin\theta/\lambda$). In each case the isotropic component of the scattering has been subtracted, and both the

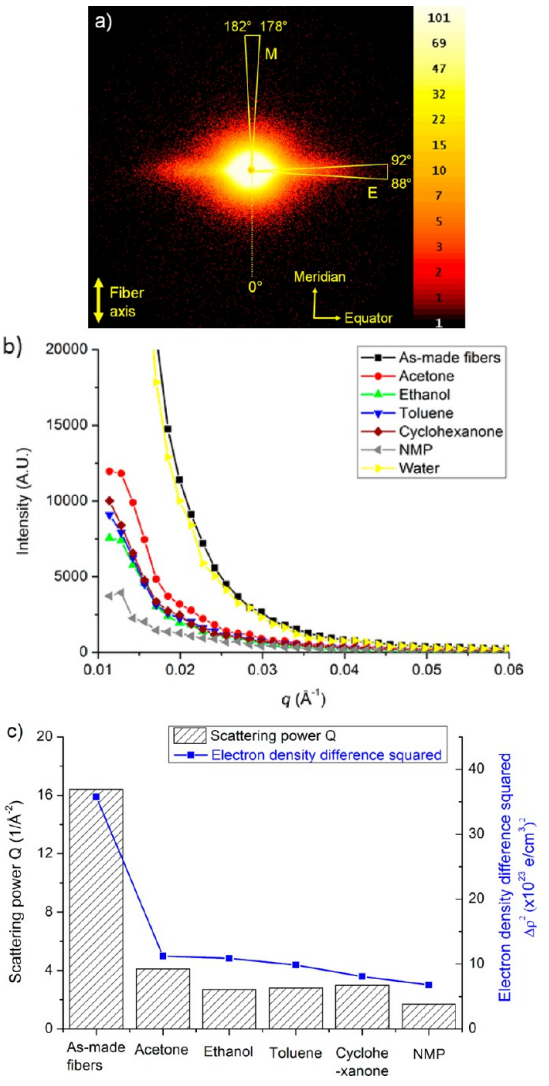

Figure 8. (a) SAXS pattern of the as-made CNT fibers, showing the equatorial fiber streak and (b) scattering intensity of the fiber streak as a function of *q* along the equator for as-made fibers and those exposed to various liquids. The fiber streak intensity was obtained from the intensity in the yellow sector E of Figure 5a from which the isotropic scattering, taken as the intensity distribution in sector M, has been subtracted. (c) Plot of the scattering power Q and calculated electron density difference squared for both as-made CNT fibers and those exposed to various liquids. The plots have been scaled to each other.

sample volume and the collection time were the same for each sample. These intensity data for each sample were the average of data collected at three different positions on the same sample. The X-ray absorption by the sample, especially in the case where liquids were involved, was corrected using the transmission coefficients before the blank was subtracted. From Figure 8b, it can be seen that the scattering intensity of the fiber streak is significantly smaller in the cases where the fiber has absorbed organic liquids on account of the reduced electron density contrast between the pores and CNT bundles. The absence of any significant reduction in intensity in the case of water is entirely

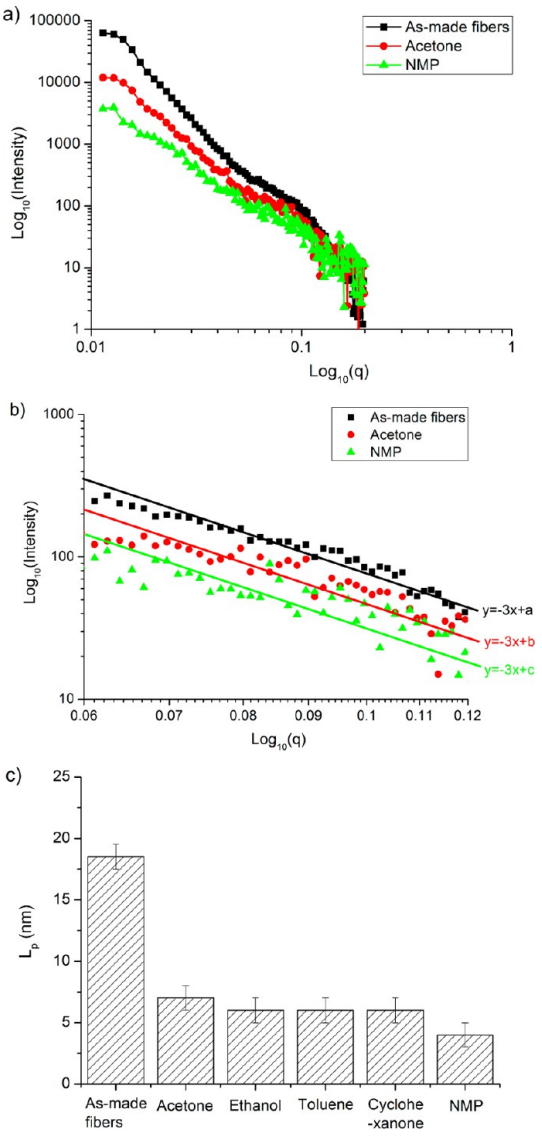

Figure 9. (a) Log−log plot of the scattering data of the fiber streak, for three cases as examples, including as-made fibers and those exposed to acetone and NMP; (b) same as (a) but for a q range of 0.06−0.12 (Å^{-1}), and the data are fitted with a linear line of slope −3; (c) bar plot representation of the lateral sizes determined using the Porod analysis.

consistent with the observation that, unlike the other liquids, water neither wets nor penetrates the fiber in liquid form. Water, although it does have some effect on electrical properties, is not considered further here.

The weighted integral of the scattered intensity along the fiber streak, the "scattering power", is a measure of the electron density difference between nanotube bundles and the voids in between, and is defined in SOM 5(i) (Supporting Information). Figure 8b shows that the reduced electron density difference in the infiltrated specimens reduces the overall intensity of the fiber streak. Figure 8c shows the scattering power scaled to calculated values for electron density difference. The measure of agreement indicates that the voids that are responsible for the scattering in the fiber streak are those that are filled by the liquid penetrant, given that possible variations in the product of volume fraction of both phases will be insignificant.

Figure 9a shows the scattering data from the fiber streak plotted as log I *vs* log q. In order to avoid overcrowding of the plot, it includes data for only three samples, as-made, acetone, and NMP, although all samples have been subject to the analysis described below. The most important observation is that for intermediate and lower scattering angles (q < 0.04 Å^{-1}), on moving from as-made to samples infiltrated with acetone and then NMP, there is a significant reduction in the slope of the scattering curve, which implies there is also a reduction in the size of the scattering bodies. The challenge is then to obtain quantitative size estimates from these data. A Guinier analysis of the lower angle data was attempted, in order to estimate a radius of gyration of the scattering entities. However, this was not entirely satisfactory because only the first few data points (close to the beam stop) satisfy the Guinier criterion that $q_{max}R_g < 1$ and second because it assumes that there is no interference function, *i.e.*, dilute solution or a function that is smeared out to be approximately constant. Instead we have chosen to analyze the weaker higher angle data, using a Porod analysis. The higher angle data are plotted on a log−log plot in Figure 9b, and the characteristic lateral sizes for the different liquids appear as a bar graph in Figure 9c. The details of this analysis, together with the results of the application of Guinier analysis, despite the shortcomings noted above, as well as an estimate of the orientation and characteristic size in the direction of the fiber axis, are given in SOM 5(ii) (Supporting Information). For the as-made sample, with a ratio of about 50:50 bundles: void, the average L_p (18 nm) becomes L_p bundles or voids 36 nm. This value is in acceptable agreement with bundle and void diameters measured from SEM, which gives a modal value of 25−30 nm; see Figure 3. One reason for the difference is that while SEM gives a number average, X-ray scattering gives a volume or weight average (more weight to larger sizes).

The overriding conclusion that can be gathered from the above measurements is that the ingress of liquids results in a marked decrease in the characteristic lateral size of the internal microstructure. The scale of the scattering entities on the as-made samples is in the same range as the SEM observation of bundles and voids in the samples. Nevertheless, there must remain questions over the exact values of these measurements in the light of the assumptions made in the analysis. However, the trends are clear, and we are confident that the relative effect of the different solvents shown in Figure 9c is meaningful. We also note that the largest effect applies in the case of NMP, known to be one of the most potent liquids for encouraging the separation of nanotubes.[11,21]

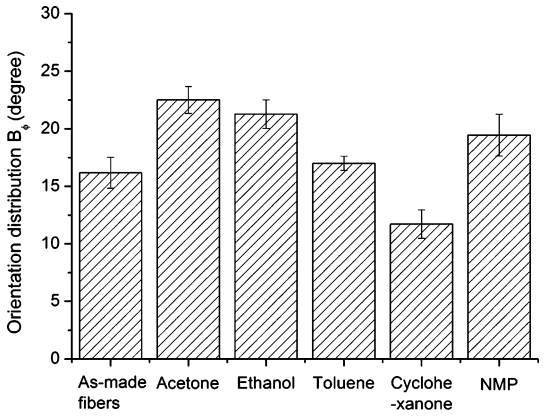

Figure 10. Plot of azimuthal width of fiber streak.

TABLE 2. List of Maximum Relative Resistance Increase and Increase Rate in Stage 2 for Fibers Immersed in Different Solvent Tested[a]

liquid	maximum resistance increase [%] (average of several runs)	increase rate [% points/sec]
NMP	38	16
cyclohexanone	21	1.2
ethanol	10	0.9
acetone	23	0.6
toluene	20 (+)	0.1
cyclohexane	20 (+)	0.1

[a] Note: For the case of nonpolar ones (toluene and cyclohexane), maximum resistance was not reached after 1 h of immersion; thus, approximate values are given.

The characteristic lateral size values derived using the Guinier analysis (Table 1 and SOM 5(ii) in Supporting Information also show this general trend).

Orientation. The azimuthal width (length of arc) of the fiber streak can be used to give an indication of the quality of alignment with the fiber axis of the diffracting entities. The main result from this analysis is that, as shown in Figure 10 with details in SOM 5(iii) (Supporting Information), the ingress of liquid leads loss of orientation of the CNT bundles (cyclohexanone is an exception). One would expect that ingress of liquid would reduce alignment, and this has been observed elsewhere.[22] However the trend with the individual liquids does not follow those of interface energies or scattering lengths, nor of characteristic lengths that are only discussed in SOM 5(iii) (Supporting Information).

Electrical Property Changes on Immersion. The CNT yarn-like fibers displayed an intriguing change in electrical resistance with time on immersion in liquid organic solvents (Figure 11 and Table 2). Since this response is related to structural changes in the fiber, it is useful both in testing the models proposed earlier and also, potentially, for future sensing applications. The electrical response was measured by mounting fibers in a 4-point DC resistance circuit (illustrated in SOM 6 in

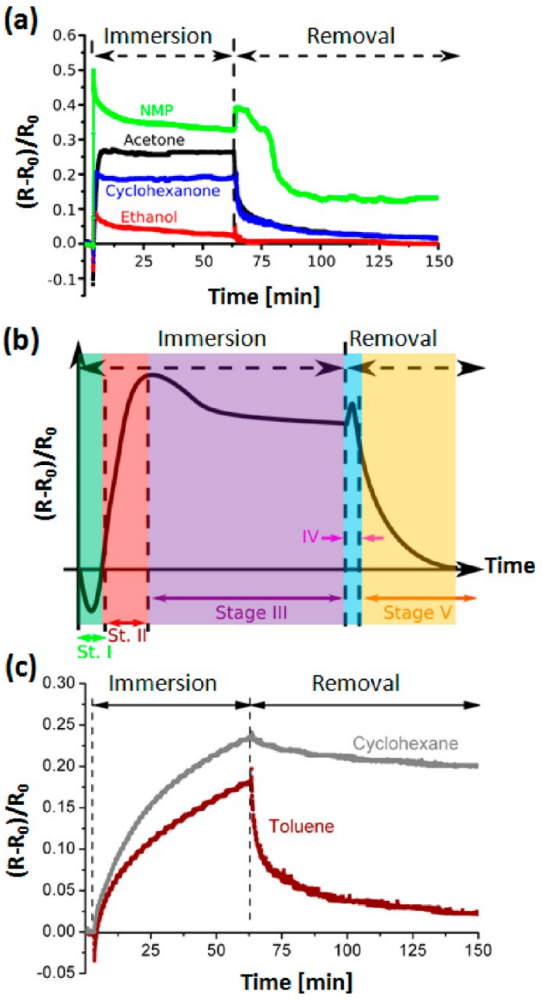

Figure 11. (a) DC resistance of CNT fiber, R, relative to original value, R_0, before immersion as function of time after immersion in a range of polar solvents: NMP, acetone, cyclohexanone and ethanol; (b) a schematic representation of the changes in relative resistance of fiber immersed in nonpolar solvents as function of time; (c) relative resistance of fiber immersed in nonpolar liquids: toluene and cyclohexane.

Supporting Information), which was then immersed into a bath of solvent. A probe current of 0.5 mA was applied, and the resistance, R, was calculated with a sampling frequency of 1 Hz, relative to the resistance of fiber before immersion, R_0. Figure 11a shows the relative resistance change, $(R - R_0)/R_0$, measured as a function of time after immersion, for a range of polar solvents. Although quantitatively different, the behavior observed was qualitatively similar for all polar solvents and shown schematically in Figure 11b, where the resistance changes have been classified in to five stages. In stage I, the resistance drops transiently as the fiber is initially immersed in the solvent. For some solvents, such as NMP, this transient response is too fast to be observed clearly in Figure 11a. Stage II involves a large increase in resistance, which occurs at different rates for the various solvents, before the resistances falls again in stage III. Stage IV is the opposite of stage I, where the

TABLE 3. List of Affinity Parameters of Air and Various Solvents toward CNTs, Together with Dipole Moment, Molar Volume, and Force Per Unit Length Exerted by Adsorbed Solvents at Junction Points Between the Nanotube Bundles (as Calculated in SOM 8 in Supporting Information)

media	affinity parameter R_δ (MPa$^{1/2}$)	dipole moment D (Debye)	molar volume V_m (cm^3 mol^{-1})	force/length (N m^{-1})
air/vapor	39.27	0	24 789.60	0.000
ethanol	13.22	1.69	58.32	0.457
toluene	10.36	0.37	105.91	0.008
acetone	6.23	2.88	74.46	0.884
cyclohexanone	4.77	2.87	103.32	0.509
NMP	2.52	4.10	97.19	1.149

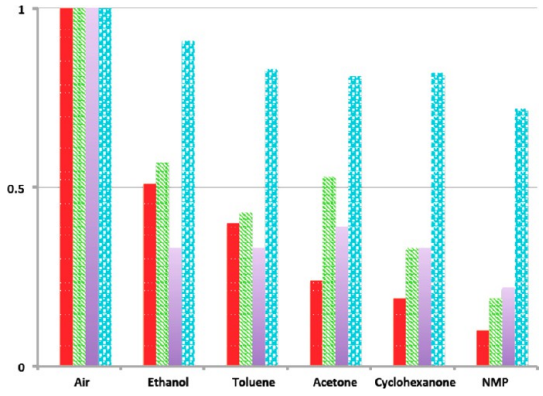

Figure 12. Plot of values of parameters measured on the CNT fibers, expressed as a ratio to the dry fiber. The order of the liquids along the horizontal axis is chosen to give a continual decrease in the Hansen affinity parameter. The color code is red, Hansen affinity parameter; green, surface energies γ_{sl}/γ_{sv}; purple, characteristic lateral size (Porod length) $L_{p,L}/L_{p,air}$; blue, reduction in conductivity σ_L/σ_{air} (or ρ_{air}/ρ_L).

resistance increases transiently as the fiber is removed from solvent, before the resistance falls again to its original value, R_0, at long times after the removal of the fiber. The behavior of two nonpolar solvents, toluene and cyclohexane, as shown in Figure 11c, differed from that of polar solvents and showed a much slower rate of resistance increase in stage II, not reaching a steady value over 1 h of immersion, before moving directly into stage IV on removal.

CONCLUSION AND STRUCTURAL MODEL

The dependence of fiber resistivity on environment is potentially of considerable significance, as this class of material is developed as a possible power and signal transmission material. In order to understand the data above, which is relevant to ingress, and the resultant structure and property effects, we will use the scheme of Hansen solubility parameters as a basis for discussion. The parameters for dispersion forces (δ_d), polar (δ_p), and hydrogen bonding (δ_h) are combined according to the following formula:

$$R_\delta = \sqrt{4(\delta_d^{NT} - \delta_d^{L})^2 + (\delta_p^{NT} - \delta_p^{L})^2 + (\delta_h^{NT} - \delta_h^{L})^2} \quad (1)$$

to give values for the affinity parameter (R_δ), the lower the value of which, the greater the level of association between the nanotubes (NT) and the solvent (L). These are given in Table 3 with the solubility parameter for air (or vapor) taken as zero. The parameter table from which these values were derived is given, with further discussion, in SOM 7 (Supporting Information).

The Hansen affinity parameters are plotted on Figure 12 (red bars) as fractions of the value for multiwall carbon nanotubes in air, with the different solvents arranged in decreasing order of this parameter. The solvent order is similar, although not the same, as that used up to now in the paper, and only solvents that have been subject to the full range of measurements are included here. Data for interface energy, lateral size of scattering entities, and resistivity reported above are also displayed in Figure 12. In each case the parameter used is expressed as a ratio to that of the dry fiber; in the case of the resistivity measurements it is the conductivity ratio that is used, to ensure that the effect of liquid ingress is expressed as a decrease. The diagram is set up to compare trends, and in particular how the magnitude of the different effects depends on the liquid used. Here, we give no weight to the fractional magnitude of the trends seen for the different types of measurement.

First, comparing the effect of the different liquids on surface energy and characteristic lateral size of scattering entities, we note that both parameters decrease on liquid ingress and that the trends broadly follow the decreasing order of the Hansen parameter, with only acetone misplaced in the order. In each case however, the most significant effect was shown by NMP. The significance of the decrease in the size of the lateral scattering entities is worthy of note. While there is, if anything, an increase in diameter of the fiber on immersion, the lateral size of the units responsible for the scattering shows a distinct decrease. We interpret this observation in terms of the breaking up of local areas in which the nanotube bundles were condensed by the online action of the acetone vapor. The bundles are presumably bent to enable the contacts to be made, where the advantage of bundle−bundle bonding energy balances the cost of elastic bending energy. Hence any liquid induced reduction in bonding energy between the bent bundles will enable them to part and the elastic distortion energy to relax. A first level model

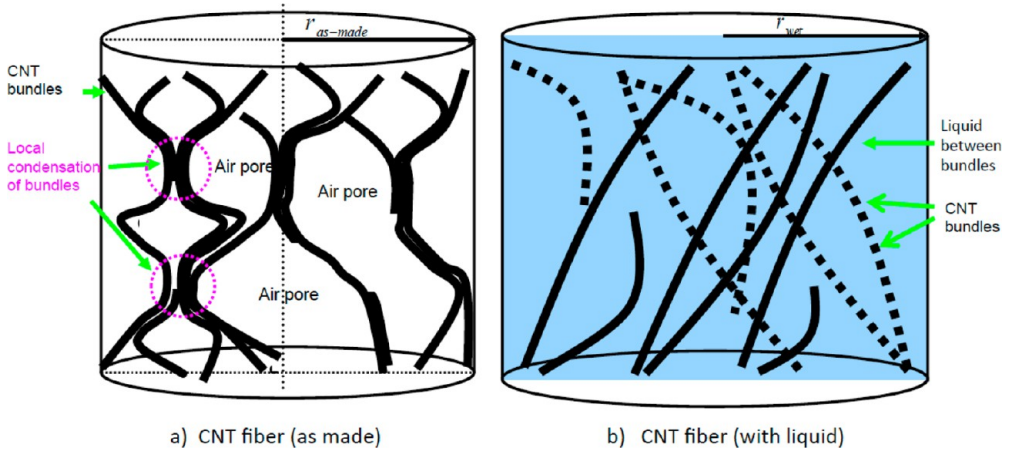

Figure 13. Schematic diagrams showing the simplified model of the structural variation of the CNT bundles within the CNT fiber both "dry" (a) and on exposure to organic liquids at room temperature (b). The degree of misorientation is exaggerated for clarity. The diagram envisages that the bundles are entangled so that the points at the top and bottom of the models are essentially fixed. In reality these entanglements will be randomly distributed throughout the fiber.

to illustrate this view forms Figure 13. We note here that a similar model was developed from small angle scattering from cellulose fibers,[22,23] where the ingress of water reduced the lateral size of the scattering entities, and subsequent small angle neutron scattering confirmed that the contrast was between water filled pores and cellulose bundles.[24] The orientation measurements, reported in Figure 10, show no distinguishable trends that might align with those seen in all the other parameters, or the Hansen values. However, as noted previously, the general trend is of some reduction in orientation on liquid ingress. Examination of the proposed model (Figure 13) would suggest that liquid absorption will decrease the alignment of some of the bundles with the fiber axis while increasing that of others. The variations seem to be larger than can be accounted for by errors implicit in the method, so we offer no explanation here but plan to return to this issue in the future.

The maximum degree by which the electrical conductivity is decreased on immersion (Figure 12, blue bars) follows the trend order in the Hansen parameters exactly, and also the nanotube/liquid interface energy and lateral size of entities fairly closely (green bars and purple bars). We interpret these effects as implying that bundle−bundle junctions are a key component of the conductivity path (given that the bundles are of limited length), so that if these junctions are broken as a result of liquid ingress, then a conductivity decrease is to be expected. Immediately on immersion there is an apparent transient increase in conductivity (apparent as a drop in resistivity in Figure 11b, stage I), irrespective of the rate at which the conductivity then begins to decrease. We explain this as the consequence of the formation of an adsorbed layer on the walls of the readily accessible nanotube bundles, which increase the capacitance, and the addition flow of charge into the fiber registers as a transient conductivity increase. Once the conductivity reaches a minimum it then tends to show a gradual recovery toward the value for the dry fiber. We consider this to be the result of relaxation of the internal structure with time but have no suggestion of an exact mechanism at this point. Once the fiber is removed from the liquid, there is a reversal of trends as the fiber loses its liquid burden by evaporation, and exactly the original conductivity is regained (stages IV and V). This drying process of course produces a similar effect to the final stages of the original fiber condensation carried out on line using acetone. While it can be seen that the maximum decreases in conductivity are relatively similar, to within a factor of 3−4, the rates of decrease vary much more widely, by up to 2 orders of magnitude (Table 2), with the two slowest ones coming from the two nonpolar solvents. It appears that the rate of increase does not follow the trends already considered, and it is apparent that the two slowest ones (by nearly an order of magnitude) are from the two nonpolar solvents. Indeed, the rate of conductivity decrease appears to be related to the polarity of the solvent per unit molar volume.

While it is obviously energetically favorable for liquid to move into bundle−bundle junctions and cause separation, with the new interface energy being lower than the sum of the graphene−graphene interface energy and the elastic bending of the nanotube bundles that enables the contact to be made, the process of liquid ingress must involve a measure of thermal activation, as the graphene−graphene bond needs to be broken in order to provide sufficient space into which the liquid molecule can move. In other words there will be an activation barrier. We propose that the absorbed layers at the tip of the "crack", which must propagate to separate the bundles, provide a mutual comparatively long-range repulsion that will reduce the activation energy for

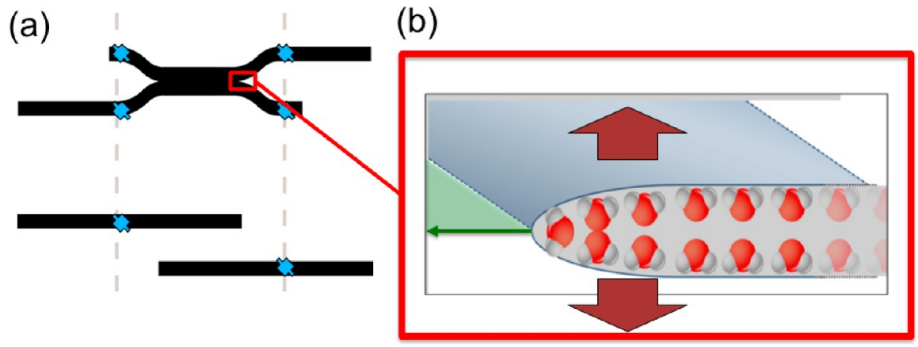

Figure 14. (a) 2D schematic representation of fiber bundle structure; (b) close up of region showing tip of liquid penetrating between graphene−graphene layers.

separation as illustrated in Figure 14. Calculations (SOM 8 in Supporting Information) indicate that the repulsive force is of a magnitude to significantly influence the size of the activation energy hump that has to be thermally surmounted. Proof of this conjecture, however, must await future experiments in which the temperature dependence of the effect is measured.

METHODS

CNT materials used in this work were synthesized by the floating catalyst chemical vapor deposition (CVD) process,[6] which involved the coinjection of methane gas, ferrocene, thiophene vapor, and hydrogen gas into a ceramic furnace tube. The overall reaction temperature was set at 1300 °C, and the "CNT aerogel" was continuously drawn from the end of the vertical furnace and wound directly onto a rotating winder at a rate of 33 m/min after being condensed using acetone spraying to produce CNT fibers. Arrays of CNT bundles can also be produced by repeatedly depositing CNTs on a rotating frame without applying the acetone mist. The internal structure of the as-spun CNT fibers was characterized using a FEI Helios Nanolab dual-beam (SEM/FIB) microscope, whereas nitrogen absorption apparatus (Micromeritics TriStar 3000 Instrument) and Pycnometer (Micromeritics Automatic Pycnometer) were used together to measure the surface area and porosity of the fiber. Thermo-Gravimetric Analysis (TA Instruments Q500 TGA) was used to quantify the impurity level of CNT fibers. The wetting properties of CNT materials toward various liquids were studied using a KSV CAM200 optical contact angle meter (KSV Instruments, Ltd., Fin-00380 Finland) at room temperature. By controlled dispensing of the liquid droplet through a syringe needle onto an aligned array of CNT bundles, the wetting and wicking of the organic liquids on the CNT array were captured by a digital camera with acquisition rate of 25 frames per second. The captured images were analyzed using CAM 200 and Image J software to obtain the contact angle and contact length of the liquid on the material, respectively. Drop sizes of 10 and 15 μL were used for organic liquids and water, respectively, with a dispensing rate of 1 μL/s in both cases. In order to study the effect of liquid infiltration on overall fiber diameter, we measured the diameter of the CNT fiber at targeted positions before and during immersion in NMP and toluene using an optical microscope (XPL 3230, Guangdong). A Textechno Favimat fiber tester was used to examine the effect of liquid contact on the fiber length. Samples were mounted vertically between top and bottom grips with an initial gauge length of 20 mm and then strained until certain load was reached. A droplet of the desired liquid was poured over the lower clamp, wetting the sample, and the drop in load, corresponding to an elongation of the fiber, was registered. WAXS data were collected in reflection mode using a D 8 diffractometer with a Cu Kα source on an as-made aligned array of CNT bundles and the same array exposed to liquids. SAXS data were collected in a Bruker Nanostar (Cu Kα) at its highest resolution (sample to detector calibrated distance 1050 mm). Fibers were examined dry and immersed in liquids held in Lindemann glass capillaries. Each fiber was examined in 3 different positions measuring both SAXS data and the transmission coefficient with a glassy carbon. Blanks were measured for the dry setup and with liquid filled capillaries for the as-made and wet samples, respectively. After correction for the differences in transmission, the blank was subtracted from the sample data, and the data sets from each of the 3 positions were averaged. Four-point DC electrical measurements were performed by means of a custom built measuring device and data logger consisting of a current regulated power supply capable of delivering from 0.001 to 2.000 $\pm$ 0.1% mA and a voltmeter with a sensitivity of 1 mV. The data were logged at 1 Hz. Fiber specimens were mounted in 50 $\times$ 20 $\times$ 3 mm PTFE specimen holders (SOM 6 in Supporting Information) with indium-based liquid-proof electrical contacts and subjected to several immersion-removal cycles in different liquids.

Conflict of Interest: The authors declare no competing financial interest.

Acknowledgment. The authors wish to thank the Cambridge Overseas Trust, Department of Materials Science and Metallurgy, Cambridge University, Dyson Ltd., and Ms. Norma Olvera for generous financial support, and Professor Ulrich Steiner of the Cavendish Laboratory Cambridge for access to contact angle equipment.

Supporting Information Available: Porosity, surface area, and composition analysis of the CNT material, relevant SAXS results, wetting and wicking results, and determination of Hansen affinity parameters between CNTs and liquids. This material is available free of charge *via* the Internet at http://pubs.acs.org.

REFERENCES AND NOTES

1. Yu, M. F.; Lourie, O.; Dyer, M. J.; Moloni, K.; Kelly, T. F.; Ruoff, R. S. Strength and Breaking Mechanism of Multiwalled Carbon Nanotubes Under Tensile Load. *Science* **2000**, *287*, 637–640.
2. Yu, M. F.; Files, B. S.; Arepalli, S.; Ruoff, R. S. Tensile Loading of Ropes of Single Wall Carbon Nanotubes and Their Mechanical Properties. *Phys. Rev. Lett.* **2000**, *84*, 5552–5555.
3. Poulin, P.; Vigolo, B.; Launois, P. Films and Fibers of Oriented Single Wall Nanotubes. *Carbon* **2002**, *40*, 1741–1749.
4. Zhang, M.; Atkinson, K. P.; Baughman, R. H. Multifunctional Carbon Nanotube Yarns by Downsizing an Ancient Technology. *Science* **2004**, *306*, 1358–1361.

5. Ericson, L. M.; Fan, H.; Peng, H.; Davis, V. A.; Zhou, W.; Sulpizio, J.; Wang, Y.; Booker, R.; Vavro, J.; Guthy, C.; et al. Macroscopic, Neat, Single-Walled Carbon Nanotube Fibers. *Science* **2004**, *305*, 1447–1450.
6. Li, Y. L.; Kinloch, I. A.; Windle, A. H. Direct Spinning of Carbon Nanotube Fibers from Chemical Vapor Deposition Synthesis. *Science* **2004**, *304*, 1215–1219.
7. Koziol, K.; Vilatela, J.; Moisala, A.; Motta, M.; Cunniff, P.; Sennett, M.; Windle, A. High-Performance Carbon Nanotube Fiber. *Science* **2007**, *318*, 1892–1895.
8. Boncel, S.; Sundaram, R. M.; Windle, A. H.; Koziol, K. K. K. Enhancement of the Mechanical Properties of Directly Spun CNT Fibers by Chemical Treatment. *ACS Nano* **2011**, *5*, 9339–9344.
9. Fan, X.; Dickey, E. C.; Eklund, P. C.; Williams, K. A.; Grigorian, L.; Buczko, R.; Pantelides, S. T.; Pennycook, S. J. Atomic Arrangement of Iodine Atoms Inside Single-Walled Carbon Nanotubes. *Phys. Rev. Lett.* **2000**, *84*, 4621–4624.
10. Zhao, Y.; Wei, J.; Vajtai, R.; Ajayan, P. M.; Barrera, E. V. Iodine Doped Carbon Nanotube Cables Exceeding Specific Electrical Conductivity of Metals. *Nature* **2011**, *83*, 1–5.
11. Bergin, S. D.; Nicolosi, V.; Streich, P. V.; Giordani, S.; Sun, Z.; Windle, A. H.; Ryan, P.; Niraj, N. P. P.; Wang, Z. T. T.; Carpenter, L.; et al. Towards Solutions of Single-Walled Carbon Nanotubes in Common Solvents. *Adv. Mater.* **2008**, *20*, 1876–1881.
12. Hernandez, Y.; Nicolosi, V.; Lotya, M.; Blighe, F. M.; Sun, Z.; De, S.; McGovern, I. T.; Holland, B.; Byrne, M.; Gunko, Y. K. et al. High-yield Production of Graphene by Liquid-Phase Exfoliation of Graphite. *Nat. Nanotechnol.* **2008**, *3*, 563–568.
13. Motta, M.; Moisala, A.; Kinloch, I. A.; Windle, A. H. High Performance Fibers from 'Dog Bone' Carbon Nanotubes. *Adv. Mater.* **2007**, *19*, 3721–3726.
14. Motta, M.; Moisala, A.; Kinloch, I. A.; Premnath, V.; Pick, M.; Windle, A. H. The Parameter Space for the Direct Spinning of Fibers and Films of Carbon Nanotubes. *Phys. E* **2007**, *37*, 40–43.
15. Wang, S.; Zhang, Y.; Abidi, N.; Cabrales, L. Wettability and Surface Free Energy of Graphene Films. *Langmuir* **2009**, *25*, 11078–11081.
16. Haynes, W. M.; Lide, D. R. *Handbook of Chemistry and Physics*, 92th ed.; CRC Press by Taylor & Francis Group: Boca Raton, FL, 2011−2012.
17. Pavese, M.; Musso, S.; Bianco, S.; Giorcelli, M.; Pugno, N. An Analysis of Carbon Nanotube Structure Wettability Before and After Oxidation Treatment. *J. Phys.: Condens. Matter* **2008**, *20*, 474206–1−7.
18. Davies, R. J.; Riekel, C.; Koziol, K. K.; Vilatela, J. J.; Windle, A. H. Structural Studies on Carbon Nanotube Fibers by Synchrotron Radiation Micro-Diffraction and Micro-Fluorescence. *J. Appl. Crystallogr.* **2009**, *42*, 1122–1128.
19. Vilatela, J. J. Structure, Properties and Treatments of Carbon Nanotube Fibers. PhD Thesis, University of Cambridge, 2009; pp 65−74.
20. Roe, R. J. *Methods of X-ray and Neutron Scattering in Polymer Science*; Oxford University Press: Oxford, U.K., 2000; pp 28−29.
21. Giordani, S.; Bergin, S. D.; Nicolosi, V.; Lebedkin, S.; Kappes, M. M.; Blau, W. J.; Coleman, J. N. Debundling of Single-Walled Nanotubes by Dilution: Observation of Large Populations of Individual Nanotubes in Amide Solvent Dispersions. *J. Phys. Chem. B* **2006**, *110*, 15708–15718.
22. Vickers, M. E.; Briggs, N. P.; Ibbett, R. N.; Payne, J. J.; Smith, S. B. Small Angle X-Ray Scattering Studies on Lyocell Cellulosic Fibers: The Effects of Drying, Re-wetting and Changing Coagulation Temperature. *Polymer* **2001**, *42*, 8241–8248.
23. Crawshaw, J.; Bras, W.; Mant, G. R.; Cameron, R. E. Simultaneous SAXS and WAXS Investigations of Changes in Native Cellulose Fiber Microstructure on Swelling in Aqueous Sodium Hydroxide. *J. Appl. Polym. Sci.* **2002**, *83*, 1209–1218.
24. Crawshaw, J.; Vickers, M. E.; Briggs, N. P.; Heenan, R. K.; Cameron, R. E. The Hydration of TENCEL® Cellulose Fibers Studied Using Contrast Variation in Small Angle Neutron Scattering. *Polymer* **2000**, *41*, 1873–1881.